Space charge influence on the angle of conical spikes developing on a liquid-metal anode

G. Sh. Boltachev,* N. M. Zubarev,† and O. V. Zubareva‡

Institute of Electrophysics, Russian Academy of Sciences, Ural Division, 106 Amundsen Street, 620016 Ekaterinburg, Russia

The influence of the space charge of ions emitted from the surface of a conical spike on its shape has been studied. The problem of the calculation of the spatial distributions of the electric field, ion velocity field, and the space charge density near the cone tip has been reduced to the analysis of a system of ordinary differential equations. As a result of numerical solution of these equations, the criterion for the balance of the capillary and electrostatic forces on the conic surface of a liquid-metal anode has been determined. It has allowed us to relate the electrical current flowing through the system, the applied potential difference, and the cone angle. We have compared the results of our calculations with available experimental data concerning emission from the surface of pure liquid gallium, indium, tin, and some liquid alloys, such as Au+Si, Co+Ge, and Au+Ge. On the basis of the proposed model, explanations have been given for a number of specific features of the emissive behavior of different systems.

I. INTRODUCTION

It is known that, as a result of the development of an electrohydrodynamic instability, the surface of a conducting liquid (liquid metal) takes the shape of a cone in a rather strong external electric field [1–7]. An enhancement of the field near the cone tip provides conditions for the initiation of emission processes such as field evaporation of ions [8–12]. Interest in studying the geometry of such structures was stimulated in large measure by the development of liquid-metal ion sources (LMISs). Considerable progress in the theory of conical spikes started from Taylor's investigations [2,13]. He has shown that, for a cone with a half angle of $\alpha_T \simeq 49.3°$, the surface electrostatic pressure P_E depends on the distance from its apex as R^{-1} and, hence, can be counterbalanced by the surface pressure $P_L \sim R^{-1}$.

The geometry of ion-emitting cones (Taylor cones) has been investigated in numerous experimental works [14–19]. These works testify that an increase in the applied potential difference is accompanied not only by the appearance and increase of the emission current, but also by a decrease of the cone half angle. For small currents, i.e., when the space charge influence is negligible, the half angle is close to Taylor's angle α_T. The phenomenon of cone sharpening can be interpreted as the system response aimed at the conservation of the balance of the pressures P_E and P_L under the conditions of the screening effect of the space charge. The last effect in the case of an emitter with invariable shape, as is known [20,21], reduces to the Child-Langmuir law.

Simple analytic models, which relate the basic parameters of a problem, play an important role in gaining insight into the physical processes that occur in liquid-metal ion sources. Among these models are Mair's theory [22], the models by Kingham and Swanson [10] and Mair and Forbes [23,24], and, certainly, Taylor's model [2]. Nevertheless, the above-

listed models do not present a theoretical description of the current dependence of the cone angle. In this work, we propose a model, which generalizes, on the one hand, Taylor's solution to the case where the space charge starts playing an important part, and, on the other hand, the Child-Langmuir law to the case of an emitter of variable (self-adjusting) shape. It is based on self-similar solutions for a charged particle flow [25,26], which were found to be compatible with the Laplace-Young stress condition for a liquid conducting cone: see our Letter [27]. Clearly, this model does not attempt to describe all the features of operation of liquid-metal ion sources. The application of self-similar solutions restricts our analysis to a precisely conical shape of the emitter. So possible deformations of the emitting cone observed in experiments, in particular, the appearance of small jetlike protrusions on its vertex, remain beyond the scope of this paper. The advantage of the proposed model is the possibility to describe distributions of the electric field potential and of the ion velocity field over the cone and, as a consequence, to obtain relations between the cone angle, the current, and the applied voltage.

II. INITIAL EQUATIONS; SELF-SIMILAR REDUCTION

Let us consider a single-velocity flow of ions evaporating from the surface of an infinite conical anode in the framework of the hydrodynamic description [25–28]. Figure 1 shows the geometry of the problem and the notations used. The mass and charge densities are proportional to each other for a charged-particle flow, and vorticity of the flow is conserved in a potential electric field ($\mathbf{E} = -\boldsymbol{\nabla}\Phi$). We assume the initial ion velocity to be equal to zero. This approximation can be considered to be well founded in view of the extremely high values of electric field strength near the cone tip. Then the vorticity of the flow is zero close to the anode surface, and, hence, the ion flow is potential. In this case, the flow velocity, along with the electric field, can be described with the help of a scalar function, the velocity potential: $\mathbf{v} = \boldsymbol{\nabla}\Psi$. Then the original set of equations can be written as follows:

*grey@iep.uran.ru
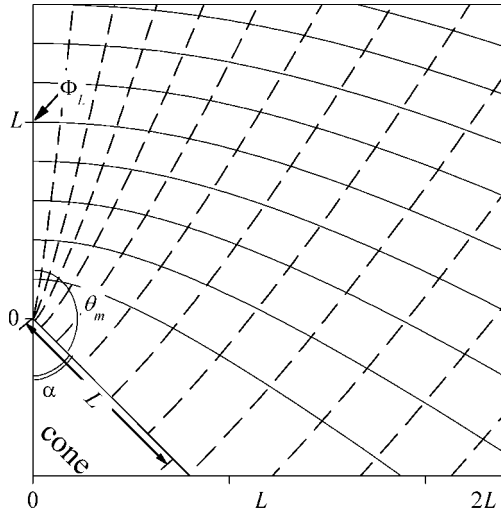†nick@ami.uran.ru
‡olga@ami.uran.ru

FIG. 1. The geometry of the problem and the notation: L is the characteristic spatial scale, α is the cone half angle, $\theta_m \equiv \pi - \alpha$, and Φ_L is the absolute value of the electric field potential at the symmetry axis at a distance L from the apex of the cone. The solid lines correspond to equipotential surfaces, including the surface of the cone with $\Phi = 0$. The dashed lines correspond to the streamlines of the ion flow.

$$\nabla^2 \Phi = -qN/\varepsilon_0, \qquad (1)$$

$$m(\nabla \Psi)^2/2 = -q\Phi, \qquad (2)$$

$$\boldsymbol{\nabla}(N \boldsymbol{\nabla} \Psi) = 0. \qquad (3)$$

The first equation is the Poisson equation for the electric field potential Φ; here N is the charged particle density, q is the particle charge, and ε_0 is the vacuum permittivity. The motion of particles is described by the second equation, which gives the energy conservation law for ions in an electric field (Ψ is the velocity potential, m is the mass of a particle). The third equation is the continuity equation. The Poisson equation (1) has to be solved together with the condition that the conductor surface is equipotential. It is convenient to take the electric potential of the the anode be equal to zero, $\Phi = 0$, which agrees with the condition that the initial velocity of particles is zero, $\boldsymbol{\nabla}\Psi = \mathbf{0}$ [see Eq. (2)].

The equilibrium configuration of the free liquid-metal surface is determined by the balance condition for the electrostatic and capillary forces (the Laplace-Young equation). For a conical surface it takes the form

$$P_L = \frac{\sigma}{R}\cot \alpha = \frac{\varepsilon_0}{2}(\nabla \Phi)^2_{\Phi=0} = P_E, \qquad (4)$$

where α is the cone half angle, σ is the surface tension, and R is the distance from the cone apex. In the case of a high mass flow rate, characteristic for the so-called cone-jet mode of electrosprays [29,30] or for sonic sprays [31], the hydrodynamic term also contributes to the pressure balance condition. However, for the process of field evaporation of ions realized in the experiments [14–19], this term appears to be

2–3 orders of magnitude smaller than the electrostatic (P_E) and capillary (P_L) terms [3], and we can neglect it.

In order to pass to dimensionless variables, we introduce some characteristic spatial scale L, which will be taken as the unit of length (see Fig. 1). Since Eqs. (1)–(3) do not have their own characteristic spatial size (they are invariant with respect to scaling), the value of L cannot be defined from the model. Below we will treat L as the size of the top part of an infinite model cone; the emission current from this part of the cone will be identified with the experimental current from a liquid-metal ion source. As an external control parameter, we introduce the absolute value of the electric field potential at the symmetry axis at the same distance L from the apex of the cone, $\Phi_L > 0$. Then it is convenient to define the dimensionless variables in the following way:

$$r = R/L, \quad \phi = -\Phi/\Phi_L,$$

$$n = NL^2q/(\varepsilon_0\Phi_L), \quad \psi = \Psi[m/(2qL^2\Phi_L)]^{1/2}, \qquad (5)$$

and the initial Eqs. (1)–(3) take the form

$$\nabla^2\phi = n, \quad (\nabla\psi)^2 = \phi, \quad \boldsymbol{\nabla}(n\boldsymbol{\nabla}\psi) = 0. \qquad (6)$$

Switching to spherical coordinates and taking into consideration the axial symmetry of the problem, we obtain

$$\phi_{rr} + \frac{2}{r}\phi_r + \frac{1}{r^2}\phi_{\theta\theta} + \frac{\cot\theta}{r^2}\phi_\theta = n,$$

$$\psi_r^2 + \frac{1}{r^2}\psi_\theta^2 = \phi,$$

$$n_r\psi_r + \frac{n_\theta\psi_\theta}{r^2} + n\left(\psi_{rr} + \frac{2}{r}\psi_r + \frac{\psi_{\theta\theta}}{r^2} + \frac{\cot\theta}{r^2}\psi_\theta\right) = 0. \quad (7)$$

It can readily be seen that these equations are invariant under the scale transformations

$$\phi \rightarrow \phi s^\gamma, \quad n \rightarrow n s^{\gamma-2},$$

$$\psi \rightarrow \psi s^{\gamma/2+1}, \quad r \rightarrow rs, \qquad (8)$$

where γ and s are some constants. Consequently, the system (7) can be reduced by means of the following self-similar ansatz (see also [25,26]):

$$\phi = r^\gamma A(\theta), \quad n = r^{\gamma-2}B(\theta), \quad \psi = r^{\gamma/2+1}C(\theta), \qquad (9)$$

where A, B, and C are unknown functions of the polar angle θ.

In the dimensionless form, the pressure balance condition (4) reads

$$(\nabla\phi)^2_{\phi=0} = \frac{\cot\alpha}{rV^2}, \quad V \equiv \Phi_L\sqrt{\frac{\varepsilon_0}{2L\sigma}}. \qquad (10)$$

The dimensionless group V plays the role of an external control parameter of the problem. One can see from this expression that the electric potential has to depend on the distance r as $\phi \sim r^{1/2}$ that uniquely determines the value of the self-similarity parameter $\gamma = 1/2$ [2,13]. Thus, we should apply the substitution

$$\phi(r, \theta) = r^{1/2} A(\theta),$$

$$n(r, \theta) = r^{-3/2} B(\theta),$$

$$\psi(r, \theta) = r^{5/4} C(\theta), \tag{11}$$

which provides separation of variables in (7). The substitution (11) enables us to reduce the partial differential equations (7) to the following set of second-order ordinary differential equations for the angular distribution of $A(\theta)$, $B(\theta)$, and $C(\theta)$:

$$(3/4)A + A_{\theta\theta} + A_\theta \cot \theta = B,$$

$$(25/16)C^2 + C_\theta^2 = A,$$

$$(15/16)BC + B_\theta C_\theta + BC_{\theta\theta} + BC_\theta \cot \theta = 0. \tag{12}$$

Note that the last equation can be simplified by introducing an auxiliary function $D(\theta) \equiv BC_\theta \sin \theta$:

$$D_\theta C_\theta = -(15/16)DC. \tag{13}$$

Solutions of Eqs. (12) must satisfy a number of conditions at the symmetry axis ($\theta = 0$) and on the cone surface ($\theta = \theta_m \equiv \pi - \alpha$):

$$A(0) = 1, \quad C_\theta(0) = 0, \quad A(\theta_m) = 0. \tag{14}$$

Note that the condition that the initial velocities of emitted particles are equal to zero, i.e., the pair of conditions $C(\theta_m) = 0$ and $C_\theta(\theta_m) = 0$, follows from the second equation of the set (12). Differentiating the same equation with respect to θ, we find that the condition $A_\theta(0) = 0$ is satisfied if the second derivative of the function $C(\theta)$ is finite at the symmetry axis. So the solution of the problem (12) and (14) is unique for a given value of θ_m.

The additional boundary condition

$$A_\theta(\theta_m) = -V^{-1}\sqrt{\cot \alpha}, \tag{15}$$

resulting from the pressure balance condition (10), is not used in seeking a solution of Eqs. (12). It allows us to determine the value of the parameter V that corresponds to the angle θ_m. Now, let us rewrite this condition in the following form:

$$V = \sqrt{\cot \alpha}/E(\alpha), \quad E(\alpha) \equiv -A_\theta(\theta_m). \tag{16}$$

The function $E(\alpha)$ defines the dimensionless value of the electric field strength on the cone surface at a distance $r=1$ from the apex $[E(\alpha) = |\nabla \phi|_{r=1, \theta=\theta_m}]$.

The intensity of the ion flux can be characterized by the electrical current I (in dimensional form) flowing through the sphere of radius L with a center at the apex of the cone:

$$I = 2\pi q L^2 \int_0^{\theta_m} N\Psi_R \sin \theta \, d\theta. \tag{17}$$

As a corresponding dimensionless quantity, it is convenient to take the group

$$J \equiv I \frac{\sqrt{m}}{(32q^2\varepsilon_0 L^3 \sigma^3)^{1/4}}, \tag{18}$$

which does not contain the potential difference Φ_L. It can be expressed in terms of the functions B and C by the following relation:

$$J = V^{3/2} F(\alpha), \quad F(\alpha) \equiv \frac{5\pi}{2} \int_0^{\theta_m} BC \sin \theta \, d\theta. \tag{19}$$

The function $F(\alpha)$ defines the particle flux from the top part of the cone, $0 < r < 1$.

The self-similar solutions (11) give the ion flux density ($j \sim n|\nabla \psi|$) and the electric field intensity ($|\nabla \phi|$) proportional to $r^{-5/4}$ and, respectively, to $r^{-1/2}$. This corresponds to a power law between the quantities j and $|\nabla \phi|$ on the cone surface,

$$j \sim |\nabla \phi|^{5/2}. \tag{20}$$

It correctly reflects the basic property of the system, namely, the nonlinear growth of current density with increasing intensity. Nevertheless, the 5/2 power law certainly differs from the exponential dependence determined by the kinetics of the field evaporation process [32].

Our solutions would be exact if the actual relation between the flux density and the electric field were the same as the model relation (20). Note that the self-similar solutions corresponding to the model law of emission (20) are the only solutions consistent with our main assumption that the surface of a liquid metal is conical. Any distinction of the law of emission from the model law (20) will lead to deviation of the surface from the ideal cone.

However, it is known from the experiments [14–19] that the surface takes a near-conical shape, and it is possible to associate it with a certain cone half angle α (the method of angle measurement is given in the above-mentioned papers). That is, the details of the current density distribution over the emitter surface (basically, ions evaporate from the protrusion growing at the cone apex) have a relatively small influence on the balance between the electrostatic and capillary forces at the periphery of the cone structures. The reason is that the influence of the space charge has an integral character (this phenomenon is most conspicuous in planar geometry, where the screening effect of the space charge in principle does not depend on its distribution). As a consequence, our approach, not claiming to describe the LMIS operation in detail, is rather applicable for the analysis of the integral (averaged) characteristics of LMISs, including the relations between the cone half angle α, the total emission current J, and the applied voltage V. The relations between these main model parameters are determined by the expressions (16) and (19). In the next section, the set of Eqs. (12) will be solved numerically. It will allow us to find the auxiliary functions $E(\alpha)$ and $F(\alpha)$, which appeared in (16) and (19). As a consequence, the dependence of α on J (V plays the role of the parameter) and the current-voltage dependence (α is the parameter) will be established.

III. CONSTRUCTION OF SOLUTIONS

A. Asymptotic expansions

In order to solve the ordinary differential equations (12) and (13) with the conditions (14) numerically, we should use asymptotic expansions for the unknown functions at $\theta \to 0$ and $\theta \to \theta_m$. This is caused by the singular behavior of the functions (or their derivatives) at the boundaries $\theta = 0$ and θ_m. As will be shown below, $B \to \infty$ at $\theta \to \theta_m$ and $B_{\theta\theta\theta} \to \infty$ at $\theta \to 0$.

At $\theta \to 0$, i.e., at the symmetry axis, the functions $A(\theta)$, $B(\theta)$, $C(\theta)$, and $D(\theta)$ can be expanded into the series

$$A = 1 + a_2\theta^2 + a_4\theta^4 + \cdots,$$

$$B = b_0\theta^\beta + b_0b_1\theta^{2+\beta} + \cdots,$$

$$C = 4/5 + c_2\theta^2 + c_4\theta^4 + \cdots,$$

$$D = d_0\theta^{2+\beta} + d_0d_2\theta^{4+\beta} + \cdots. \tag{21}$$

Substitution of these expressions into the initial Eqs. (12) and (13) yields

$$a_2 = -\frac{3}{2^4}, \quad a_4 = \frac{1}{2^{10}}, \quad \ldots,$$

$$c_2 = \frac{-5 + \sqrt{13}}{2^4}, \quad c_4 = \frac{295 - 107\sqrt{13}}{9 \times 2^{10}}, \quad \ldots,$$

$$\beta = \frac{\sqrt{13}+1}{2} \simeq 2.3, \quad b_1 = -\frac{275 + 173\sqrt{13}}{1152}, \quad \ldots,$$

$$d_0 = 2b_0c_2, \quad d_2 = -\frac{165 + 31\sqrt{13}}{384}, \quad \ldots. \tag{22}$$

The expansions (21) satisfy the two first conditions from (14); they contain a free parameter (the coefficient b_0), which is determined by the following condition at the cone surface: $A(\theta_m) = 0$. Note that the divergence of higher derivatives of the function B leads to the divergence of higher derivatives of the functions A and C. The next terms of the expansions (21) for A and C are of the order of $\theta^{2+\beta}$.

In the limit $\theta \to \theta_m$, i.e., on the cone surface, the unknown functions can be expanded into power series in the parameter $x = \theta_m - \theta$:

$$A = x^{1/2}\sum_i a_i'x^{i/2}, \quad B = x^{-1}\sum_i b_i'x^{i/2},$$

$$C = x\sum_i c_i'x^{i/2}, \quad D = d_0'\left(1 + x^{3/2}\sum_i d_i'x^{i/2}\right). \tag{23}$$

The first coefficients of these expansions are listed below:

$$a_2' = \frac{4}{3}b_1', \quad c_1' = \frac{2}{3}\sqrt{a_1'},$$

$$c_2' = \frac{1}{3}\frac{b_1'}{\sqrt{a_1'}}, \quad b_2' = -\frac{2}{3}\frac{b_1'^2}{a_1'},$$

$$d_0' = -b_1'\sqrt{a_1'}\,\sin\,\theta_m, \quad d_1' = -\frac{5}{16}. \tag{24}$$

The free parameters of these expansions, namely, the coefficients a_1' and b_1', are determined by the boundary conditions at the symmetry axis.

Increasing the charge density over the cone leads to screening of the electric field at its surface, i.e., the coefficient a_1' will approach zero. In the formal limit $a_1' = 0$ (the electric field turns to zero at the anode surface), another asymptotics is realized:

$$A = x^{1/3}\sum_i a_i''x^i, \quad B = x^{-5/3}\sum_i b_i''x^i,$$

$$C = x^{2/3}\sum_i c_i''x^i, \quad D = d_0''\left(1 + x\sum_i d_i''x^i\right), \tag{25}$$

where

$$a_1'' = \frac{9}{4}b_1'', \quad a_2'' = \frac{6}{5}b_1''\cot\theta_c,$$

$$c_1'' = \frac{9}{10}\sqrt{b_1''}, \quad c_2'' = \frac{3}{20}\sqrt{b_1''}\cot\theta_c,$$

$$b_2'' = \frac{11}{15}b_1''\cot\theta_c, \quad d_0'' = -\frac{3}{2}b_1''^{3/2}\sin\theta_c,$$

$$d_1'' = -\frac{9}{32}, \quad \ldots. \tag{26}$$

These expressions contain two free parameters: the coefficient b_1'' (or d_0'') and the angle $\theta_m \equiv \theta_c$ at which complete screening of the external field occurs.

It should be noted that the function D converges rapidly near the cone surface for both forms of expansion, (23) and (25). Therefore, using the function D is preferable to using the function B in the procedure of numerical integration of the problem (12)–(14).

B. Numerical calculations

The set of equations (12) and (13) was solved numerically by the third-order prediction-correction method. The calculation starts from the asymptotics (23) or (25). It has been found that the equations admit solutions for the angles in the range $\theta_T \leq \theta_m \leq \theta_c$. The minimum angle value $\theta_T \simeq 130.71°$ corresponds to the Taylor cone ($\alpha = \alpha_T \simeq 49.29°$) and refers to the special case of no space charge, i.e., $B = 0$. For this case, the θ dependence of A is determined by the Legendre function $P_{1/2}(\cos\theta)$. The upper bound of the angle, θ_c, is $\simeq 158.11°$. It corresponds to the least possible half angle of the cone $\alpha = \alpha_c \simeq 21.89°$. This configuration of the surface relates to the formal limit that the electric field at the cone is completely screened by the space charge (this limit cannot be achieved because of the finite emissivity of the surface). The results of the calculations, corresponding to different values of α, are presented in Fig. 2. In view of the obvious relations
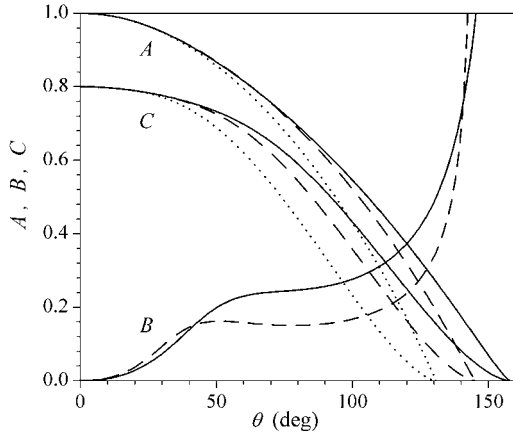
FIG. 2. Solutions of the system (12) for the cone half angles $\alpha=\alpha_T$ (dotted lines), $\alpha=35°$ (dashed lines), and $\alpha=\alpha_c$ (solid lines).

$$\nabla\phi = r^{-1/2}\{A/2, A_\theta, 0\},$$

$$\nabla\psi = r^{1/4}\{5C/4, C_\theta, 0\}, \qquad (27)$$

the angular dependences of $A(\theta)$ and $C(\theta)$ give an idea of the distributions of the electric field and the velocity field. As an example, Fig. 1 shows the equipotential surfaces and streamlines of the flow corresponding to $\alpha=45°$.

C. The electric field strength at the cone surface

The calculations show that the function $E(\alpha)$ grows monotonically from zero to the value $\simeq 0.975$ as the angle α increases from α_c to α_T (see Fig. 3). Near the limiting case (25), the estimate $E(\alpha)\sim(\alpha-\alpha_c)^{1/2}$ is valid for $\alpha\to\alpha_c$. To verify this dependence, it is possible to draw an analogy between the considered problem and the problem of a charged particle flow in a plane vacuum diode, which can be solved analytically. Actually, in the one-dimensional case,
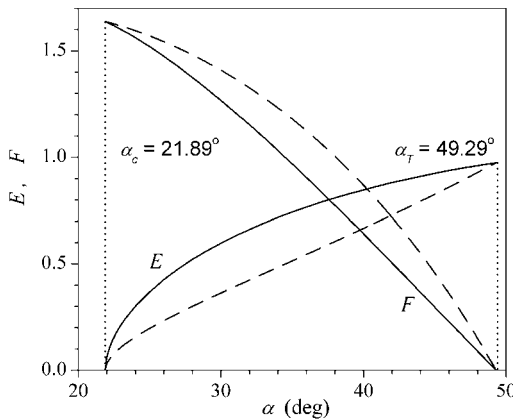

FIG. 3. Auxiliary functions $E(\alpha)$ and $F(\alpha)$ (solid lines), which represent the electric field strength on the cone surface at $r=1$ and, respectively, the ion flux from the top part of the cone ($0<r<1$). The dashed lines correspond to the one-dimensional model Eqs. (31)–(33).

where all quantities depend only on one coordinate z, Eqs. (6) reduce to the set of ordinary differential equations

$$\phi_{zz} = n, \quad \psi_z^2 = \phi, \quad (n\psi_z)_z = 0, \qquad (28)$$

which look like Eqs. (12) after the substitution $z\to\theta$. These equations admit the following exact implicit solution for the electric field potential ϕ:

$$6j^2z - E_0^3 = (2j\sqrt{\phi} - E_0^2)\sqrt{4j\sqrt{\phi} + E_0^2}, \qquad (29)$$

where $j=n\psi_z$ is the constant current density, and $E_0=\phi_z|_{z=0}$ is the electric field strength at the planar emitter. Let us also introduce the notation for the electric strength at the opposite electrode, $E_1=\phi_z|_{z=h}$ (h is the interelectrode distance), and for the electric potential on it, $\phi_h=\phi|_{z=h}$. From the solution (29) one can obtain the relations between the quantities E_0, E_1, ϕ_h, h, and j,

$$4j\sqrt{\phi_h} = E_1^2 - E_0^2,$$

$$6j^2h - E_0^3 = (2j\sqrt{\phi_h} - E_0^2)E_1. \qquad (30)$$

By analogy with θ_c, we introduce the interelectrode distance $h_c=4\phi_h/(3E_1)$, corresponding to the limit $E_0=0$, and then rewrite the expressions (30) as

$$j = \frac{4\phi_h^{3/2}}{9h_c^2}\left(1 - \frac{E_0^2}{E_1^2}\right), \quad \frac{h}{h_c} = 1 - \left(\frac{E_0}{E_1+E_0}\right)^2. \qquad (31)$$

Note that, in the limit $E_0/E_1\to 0$, the first equation of (31) represents the Child-Langmuir law [20,21] for a plane vacuum diode. It follows from the second equation of (31) that $E_0\approx E_1\sqrt{1-h/h_c}$ in the same limit, i.e., for fixed ϕ_h and E_1, the electric field strength at the emitter surface E_0 has a square root dependence on the small quantity h_c-h. For $h=h_c$, the electric field at the emitter surface is completely screened by the space charge. At given ϕ_h and E_1, the space charge density decreases as the interelectrode distance h is reduced. The opposite limit, where the space charge is absent ($E_0=E_1$ and $\phi(z)=E_1z$), is reached at $h=(3/4)h_c$.

So, in the framework of the discussed analogy we can identify (i) the angles θ_m, θ_c, and θ_T with the interelectrode distances h, h_c, and $h_T=(3/4)h_c$, respectively, (ii) the electric field strength on the cone surface at a unit distance from the apex E with the strength at the surface of the planar emitter surface E_0, (iii) the electric field strength at the symmetry axis at a unit distance from the cone apex $|\nabla\phi|=1/2$ with the strength at the opposite electrode E_1, and also (iv) the unit potential difference between the cone axis and its surface for $r=1$ with the fixed potential difference ϕ_h for a plane vacuum diode. In order to compare the characteristics of conical and planar diodes, we apply the linear mapping of the angle interval $\theta_T\leq\theta_m\leq\theta_c$ into the interval of distances $h_T\leq h\leq h_c$,

$$\frac{h-h_T}{h-h_c} = \frac{\theta_m-\theta_c}{\theta_m-\theta_T}. \qquad (32)$$

The analogs of the functions $F(\alpha)$ and $E(\alpha)$ corresponding to the one-dimensional model (28),

$$F_{\mathrm{pl}} = \frac{9jh_c^2}{4\phi_h^{3/2}}F(\alpha_c), \quad E_{\mathrm{pl}} = \frac{E_0}{E_1}E(\alpha_T), \qquad (33)$$

are presented in Fig. 3. It can be seen that the properties of conical (12) and planar (28) models are qualitatively similar. Consequently, we should expect that $E \sim (\theta_c - \theta_m)^{1/2}$ at $\theta_m \to \theta_c$, or, in terms of the cone half angle, $E \sim (\alpha - \alpha_c)^{1/2}$ at $\alpha \to \alpha_c$, as we wished to show.

Taking into account such a dependence near the limiting regime (25), we approximate the calculated dependence of E on α, by the formula

$$E(\alpha) = -0.9754\xi - 0.6176\xi^2 + 0.8342\xi^3 - 0.2164\xi^4, \tag{34}$$

where $\xi = [(\alpha - \alpha_c)/(\alpha_T - \alpha_c)]^{1/2}$. The error of the approximation (34) is less than 0.1% over the range $\alpha_c < \alpha < \alpha_T$. According to the balance condition (16), the obtained dependence $E(\alpha)$ determines the relation between the geometry of the emitting cusp, i.e., the angle α, and the external control parameter of the system, i.e., the potential $V \sim \Phi_L$.

D. The relations between model parameters

The quantity $F(\alpha)$, which is determined by (19), specifies a particle flux from the top part of the cone, $0 < r < 1$. The angular dependence of this function obtained as a result of numerical solution of the problem (12)–(14) is presented in Fig. 3. The calculated function $F(\alpha)$ can be approximated by the relation

$$F(\alpha) \simeq 1.8863\zeta + 0.0956\zeta^2 - 0.2259\zeta^3 - 0.1167\zeta^4, \tag{35}$$

where $\zeta(\alpha) = 1 - \xi^2 = (\alpha_T - \alpha)/(\alpha_T - \alpha_c)$. The error of this approximation is less than 0.15%. Note that the function $F(\alpha)$ monotonically decreases from $\simeq 1.637$ to zero as the angle α changes from α_c to α_T.

The expressions (16) and (19) together with (34) and (35) allow us to obtain the dependence of the cone half angle α on the current J as well as the current-voltage characteristic of the cone, i.e., the dependence of J on V. These relationships are plotted in Figs. 4 and 5, respectively.

From Fig. 4 it can be seen that the angle monotonically decreases with increasing current. It is equal to the Taylor angle $\alpha_T \approx 49.29°$ at zero current and tends to the angle $\alpha_c \approx 21.89°$ in the formal limit of an infinite current. Note that the interpretation of experiments [14–19] in the framework of our model corresponds to the dimensionless current in the range $0 < J < 1$ (see the inset of Fig. 4). For larger current values, the cone structure becomes unstable.

An important feature of the theoretical current-voltage characteristic (Fig. 5) is its threshold character. There is no electric current, $J = 0$, if $V < V_0 = \sqrt{\cot \alpha_T / f(\alpha_T)} \simeq 0.9512$. This is related to the impossibility of a balance between the electrostatic and capillary forces at a relatively small potential difference. The capillary force will dominate and the cone structure will break. In the formal limit of large V the model yields the universal Child-Langmuir law $J \to F(\alpha_c)V^{3/2}$, which describes the regime of space charge
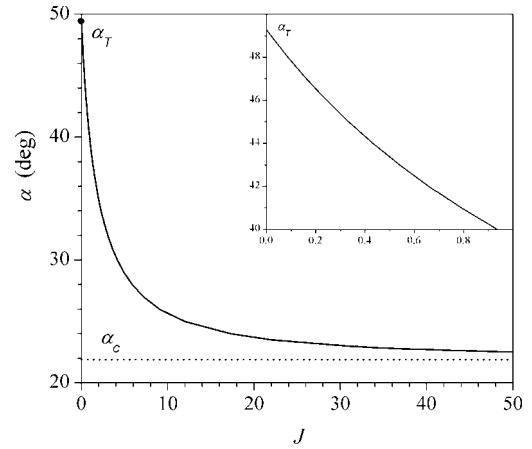

FIG. 4. Dependence of the cone half angle α on the dimensionless emission current J. The inset demonstrates the same dependence for relatively small currents.

limitation of the current as a result of complete screening of the electric field at the electrode surface.

Excluding the parameter α from (16) and (19), we can rewrite the dependence of J on V in the explicit form. The function F linearly goes up to the value $F(\alpha_c)$ as $\alpha \to \alpha_c$ (see Fig. 3), and, as discussed above, the function E tends to zero according to the square root law. As a consequence, the dependence of J on V must have the form $J \approx j_0 V^{3/2} + j_1 V^{-1/2}$ in the limit $V \to \infty$. With this estimate taken into account, for $V > V_0$ the required dependence can be approximated by the expression

$$J = V^{3/2}\left(j_0 + \frac{j_1}{V^2} + \frac{j_2}{V^4} + \frac{j_3}{V^6}\right). \tag{36}$$

The coefficients of the approximation (36) are the following: $j_0 = 1.6372$, $j_1 = -1.8635$, $j_2 = 0.3523$, $j_3 = -0.00676$; the approximation error is less than 0.00015 in absolute value.

Thus, the relations (16) and (19) together with the approximate expressions (34)–(36) completely determine the
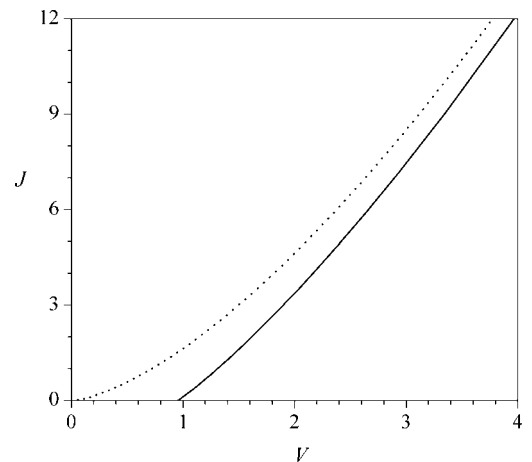

FIG. 5. Current J as a function of the applied potential difference V. The dotted line shows the asymptotic shape of the current-voltage characteristic corresponding to the Child-Langmuir law.
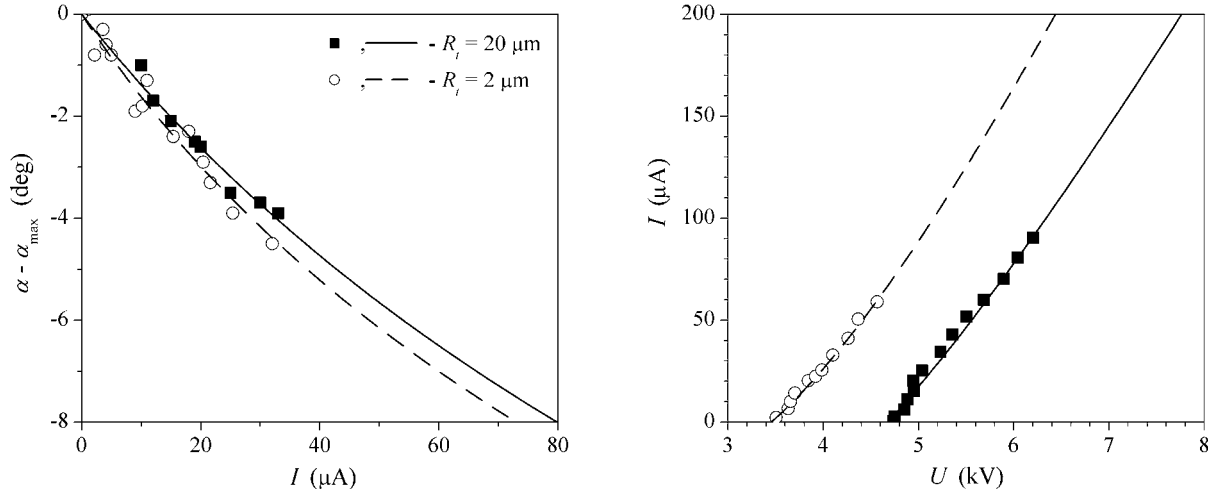
FIG. 6. Change in the cone half angle versus the emission current (left) and the current-voltage characteristics (right) for a gallium liquid-metal ion source. The points correspond to the experimental data of [15] and the lines to the theory.

integral characteristics of the system. They establish relationships between the following quantities: the applied potential difference V, the emission current J, and the cone half angle α. This will allow us to compare our theoretical calculations with available experimental data in the next section.

IV. COMPARISON WITH EXPERIMENTAL DATA

In order to compare the results of our calculations with experimental data, we assume that the control parameter of the model Φ_L is directly proportional to the potential difference U applied to the interelectrode space, i.e.,

$$\Phi_L = \kappa U, \qquad (37)$$

where the proportionality coefficient κ is determined by constructional features of an experimental facility and does not depend on the emission current. Then, after switching to dimensional quantities, the expressions (16) and (19) become

$$U = \left(\frac{2\sigma}{\varepsilon_0}\right)^{1/2} \frac{\sqrt{L(\alpha)}\cot \alpha}{\kappa E(\alpha)}, \qquad (38)$$

$$I = \varepsilon_0 \left(\frac{2q}{m}\right)^{1/2} F(\alpha)(\kappa U)^{3/2}. \qquad (39)$$

Here we take into account that the characteristic size L of the top part of the infinite model cone (the electric current from this part of the cone is identified with the emission current from the experimentally observed conical spike) can depend on the value of the emission current and, as a consequence, on the angle α.

The relations (38) and (39) together with the approximate formulas (34)–(36) allow one to determine the free parameters of the model, namely, the characteristic size of the cone $L(\alpha)$ and the coefficient κ characterizing the electric field distribution in the experimental facilities, from the available experimental data on current-voltage and current-angle dependencies for liquid-metal ion sources. We have used data for emission into vacuum from liquid indium [14], gallium

[15], and tin [17], and also from liquid alloys Au+Si [16], Co+Ge [18], and Au+Ge [19]. In our calculations we have taken the following values of the surface tension: σ =0.572 N/m (In [17]), 0.735 N/m (Ga [17]), 0.560 N/m (Sn [17]), 2.20 N/m (Au+Si [19]), 1.84 N/m (Co+Ge [18]), and 1.62 N/m (Au+Ge [19]). The angular dependence of L was approximated by the two-parameter function

$$L(\alpha) = L_c + (L_T - L_c)\left(\frac{\alpha - \alpha_c}{\alpha_T - \alpha_c}\right)^2, \qquad (40)$$

where L_T and L_c are parameters. It should be noted that the maximum half angle α_{max}, corresponding to zero emission current in the experiments [14–19], slightly differs from the Taylor angle α_T. Thus, for comparison with the theory, the experimentally observed values of α have been corrected by $\alpha_T - \alpha_{max}$.

Due to its physical properties (low temperature of melting, low pressure of saturated vapor, primarily single ionization in the emission processes), gallium is the most convenient and reliable metal for investigating the operation of liquid-metal ion sources [3]. In [15] gallium ion sources, including tungsten needles with tip radii R_t=2 and 20 μm, were investigated. As a result of treating the data on the current-voltage characteristics and geometry of the observed structures on the surface of liquid gallium, presented in [15], we obtain κ=0.0905, L_T=0.65 μm, L_c=0.84 μm (R_t =2 μm); κ=0.076, L_T=0.84 μm, L_c=0.84 μm (R_t =20 μm). The achieved quality in describing the experimental data is demonstrated in Fig. 6. Application of a sharper needle (with R_t=2 μm) provides a stronger focusing of the electric field that corresponds to a larger value of the coefficient κ and, consequently, to a smaller value of the threshold potential difference (see Fig. 6). On the other hand, a small initial radius of curvature probably begins to "constrict" the developing cone; the value of L_T corresponding to R_t=2 μm is somewhat smaller than for R_t=20 μm. According to the relations (38) and (39), a smaller size of the cone leads to faster change of the cone half angle with increase in emission current, all other parameters (the surface tension
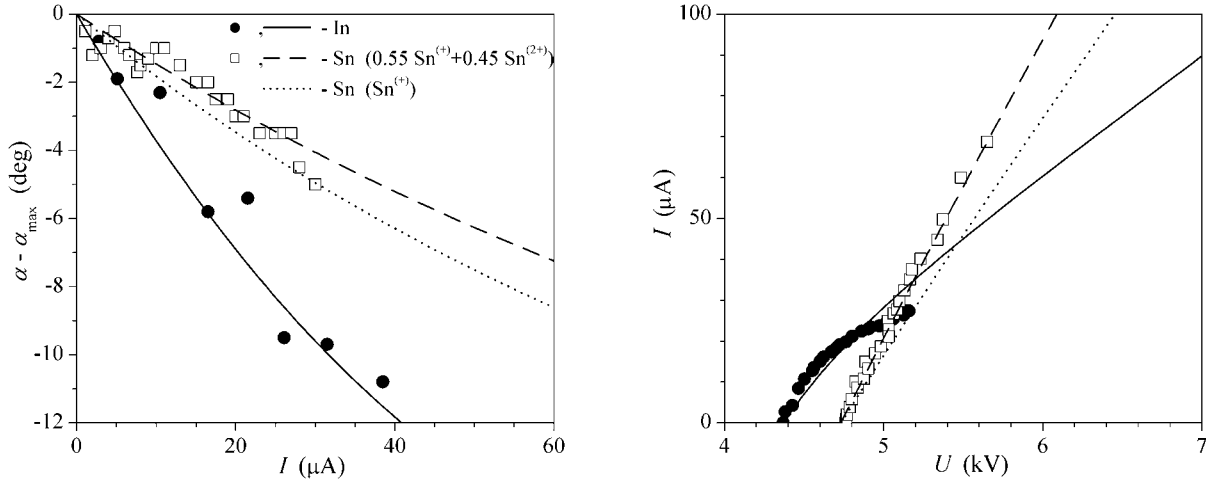
FIG. 7. Change in the cone half angle versus the emission current (left) and the current-voltage characteristics (right) for indium and tin liquid-metal sources. The points correspond to the experimental data of [14,17] and the lines to the theory; the solid line corresponds to indium, the dashed line to tin, and the dotted line to tin under the condition of the emission of singly charged ions Sn⁺ only.

coefficient, the mass and charge of emitted particles) being the same (see Fig. 6). Note that the values of L_T obtained are comparable with the size of the experimentally observed cones (they are of the order of 1 μm).

Figure 7 shows the current-voltage and current-angle dependencies for the conical spikes observed at the surfaces of liquid indium [14] and tin [17]. Probably, the strongly non-linear character of the current-voltage dependence for indium is an experimental error [14]. In later publications [18,19] the same authors approximate this dependence by a linear function; its slope is approximately the same as for the corresponding theoretical curve in Fig. 7.

It has been noted in [17] that both singly Sn⁺ and doubly charged ions Sn²⁺ are emitted from the surface of tin. The fraction of doubly charged ions is $x_2 = N_2/(N_1 + N_2) \simeq 45\%$ [19]. It is easy to verify that the relations obtained above are applicable for a flow consisting of k different types of particles. The only necessary modification refers to the expression for total current, (39). We should apply the following change:

$$\sqrt{\frac{2q}{m}} \rightarrow \sum_{i=1}^{k} \frac{q_i x_i}{Q} \sqrt{\frac{2q_i}{m_i}}, \quad Q = \sum_{i=1}^{k} q_i x_i, \quad (41)$$

where q_i, m_i, and x_i are the charge, mass, and relative fraction of particles of i type. So, for the case of tin ($q_2 = 2q_1 = 2e$, $m_2 = m_1 = m$), the expression (39) transforms into

$$I = \frac{1 + (2\sqrt{2} - 1)x_2}{1 + x_2} \varepsilon_0 \left(\frac{2e}{m}\right)^{1/2} F(\alpha)(\kappa U)^{3/2}, \quad (42)$$

where e is the elementary charge. Indium ions are emitted in the singly charged state In⁺ [19], so that such a modification is not required for an indium liquid-metal ion source. The theoretical curves presented in Fig. 7 correspond to the following values of the parameters: $\kappa = 0.0495$, $L_T = 0.4$ μm, $L_c = 0.3$ μm (In); $\kappa = 0.075$, $L_T = 1.1$ μm, $L_c = 0.78$ μm (Sn).

Indium and tin have close atomic weights and surface tension coefficients. In this connection, a sharp distinction between the dependences $I(U)$ and $\alpha(I)$ corresponding to these metals is surprising [17]. One of the likely reasons for the different behavior of indium and tin is the presence of a large amount of Sn²⁺ ions in the experiments [17]. Ions with larger charge numbers move more quickly away from the electrode and, as a consequence, provide less screening effect. Therefore, an increase in the voltage is accompanied by a larger increase in the emission current and by a relatively slow change in the cone shape. The dependences $I(U)$ and $\alpha(I)$, corresponding to the assumptions that only the singly charged ions Sn⁺ are emitted from liquid tin and the parameters κ, L_T, and L_c are fixed, are shown in Fig. 7 by the dotted line. One can see that considering only singly charged ions draws together the model the model characteristics of liquid-metal emitters based on liquid tin and indium. However, the initial difference between the curves is too large and cannot be explained only by the presence of Sn²⁺ ions.

Another reason for the behavior difference between liquid-metal ion sources is in the conditions of the experimental studies [14] and [17]. The theoretical model presented in this work points to the essential difference between the characteristic sizes L_T of the cones. One can assume that the developing cone was constricted by the small size of the tip of the tungsten needle in the experiment with indium ($R_t = 1.0$ μm according to [14]). Although the value of the tip radius $R_t = 4$ μm for the experiments with indium was indicated in the subsequent paper [19], it was measured with the help of the image of the liquid surface instead of the needle. The above analysis of gallium emitters with different needles shows that the constriction effect becomes appreciable if $R_t \lesssim 2$ μm.

Finally, Fig. 8 shows the dependencies $I(U)$ and $\alpha(I)$ for the liquid alloys Au+Si [16], Co+Ge [18], and Au+Ge [19] that correspond to the model coefficients $\kappa = 0.084$, $L_T = 1.0$ μm, $L_c = 0.45$ μm (Au+Si); $\kappa = 0.084$, $L_T = 0.27$ μm, $L_c = 0.08$ μm (Co+Ge); $\kappa = 0.051$, $L_T = 0.30$ μm, $L_c = 0.10$ μm (Au+Ge). The theory and obser-
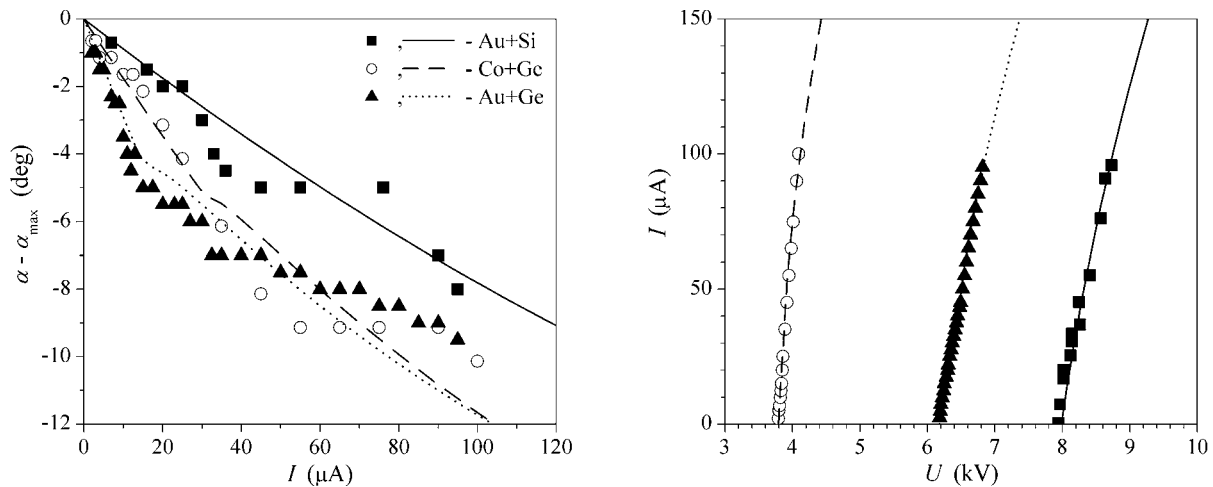
FIG. 8. Change in the cone half angle versus the emission current (left) and the current-voltage characteristics (right) for Au+Si [16], Co+Ge [18], and Au+Ge [19] alloy liquid-metal ion sources. The points correspond to the experimental data and the lines to the theory.

vations are in rather good agreement only for Au+Si from the above-listed alloys. The alloys containing germanium are distinguished by the presence of breaks on the experimental curves $\alpha(I)$. This behavior cannot be described in the framework of the proposed model. The anomalous character of the dependence $\alpha(I)$ can be caused by changing properties of the charged particle flow. So "freezing" of the cone angle along with the continuing growth of the emission current, which is characteristic for the mentioned alloys (see Fig. 8), allows us to suppose that, from some point, the average ratio of mass and charge density over the flow decreases. Unfortunately, the experimental works [18,19] does not include information about changes in the mass-to-charge ratio with the emission current. In Fig. 8 the theoretical curves are obtained under the assumption that the intense emission of doubly charged germanium ions Ge^{2+} starts at some value of the applied potential difference U_1 (or current I_1). The quantities U_1 and I_1 are of the order of 3.87 kV and 30 μA for the alloy Co+Ge, and 6.3 kV and 15 μA for Au+Ge. In both cases, the potential drop is $\Phi_L = \kappa U \simeq 0.32$ kV at a distance of the order of the cone size $(R=L)$.

V. CONCLUSION

In the present paper we have developed a self-consistent model describing how the space charge near the emitting cone apex affects its shape. Our approach is based on the self-similar reduction of the equations that govern the spatial distributions of the electric field, ion velocity field, and particle concentration to a system of ordinary differential equations. As a result of numerical solution of this system, the conditions for the mutual compensation of the capillary and electrostatic forces on the conic surface of a liquid-metal anode have been obtained. This allows us to find the depen-

dences of the cone angle and emission current on the applied potential difference. They correctly represent the main features of the operation of a liquid-metal ion source. A comparison was made between the developed theoretical model and available experimental data for emission from pure gallium, indium, and tin, or from alloys Au+Si, Co+Ge, and Au+Ge. Based on our theoretical results, we have proposed explanations for some specific features of the emissive behavior of these systems. So the difference in behavior between indium and tin, which have close characteristics (the coefficient of surface tension, the mass-to-charge ratio) is probably related to the presence of doubly charged ions Sn^{2+} in tin emission and to use of a sharper tungsten needle in the experiments with indium.

In conclusion, let us note once again that the developed model does not pretend to describe all aspects of operation of liquid-metal ion sources. In particular, the consideration of the jetlike protrusion at the cone vertex, from which the vast majority of ions are evaporated, remains beyond the scope of the model. The self-similar solutions used above describe LMIS operation in terms of the averaged characteristics (α, I, and U) only.

[1] J. Zeleny, Phys. Rev. **10**, 1 (1917).

[2] G. I. Taylor, Proc. R. Soc. London, Ser. A **280**, 383 (1964).

[3] R. G. Forbes, Vacuum **48**, 85 (1997).

[4] L. Oddershede and S. R. Nagel, Phys. Rev. Lett. **85**, 1234 (2000).

[5] N. M. Zubarev, JETP Lett. **73**, 544 (2001).

[6] N. M. Zubarev, Phys. Rev. E **65**, 055301(R) (2002).

[7] V. G. Suvorov and N. M. Zubarev, J. Phys. D **37**, 289 (2004).

[8] R. Gomer, Appl. Phys. **19**, 365 (1979).

[9] N. K. Kang and L. W. Swanson, Appl. Phys. A: Solids Surf. **30**, 95 (1983).

[10] D. R. Kingham and L. W. Swanson, Appl. Phys. A: Solids Surf. **34**, 123 (1984).

[11] G. S. Cho, Y. Seo, and S. O. Kang, J. Appl. Phys. **72**, 5892 (1992).

[12] P. Wang, S. Maheshwari, and H.-C. Chang, Phys. Rev. Lett. **96**, 254502 (2006).

[13] G. I. Taylor, Proc. R. Soc. London, Ser. A **291**, 145 (1966).

[14] B. Praprotnik, W. Driesel, C. Deitzsch, and H. Neidrig, Surf. Sci. **314**, 353 (1994).

[15] W. Driesel, C. Dietzsch, H. Niedrig, and B. Praprotnik, Ultramicroscopy **57**, 45 (1995).

[16] W. Driesel, C. Dietzsch, and R. Mühle, J. Phys. D **28**, 787 (1995).

[17] W. Driesel and C. Dietzsch, Appl. Surf. Sci. **93**, 179 (1996).

[18] W. Driesel, C. Dietzsch, E. Hesse, L. Bischoff, and J. Teichert, J. Vac. Sci. Technol. B **14**, 1621 (1996).

[19] W. Driesel, C. Dietzsch, and R. Mühle, J. Vac. Sci. Technol. B **14**, 3367 (1996).

[20] C. D. Child, Phys. Rev. **32**, 492 (1911).

[21] I. Langmuir, Phys. Rev. **2**, 450 (1913).

[22] G. L. R. Mair, J. Phys. D **17**, 2323 (1984).

[23] G. L. R. Mair and R. G. Forbes, J. Phys. D **24**, 2217 (1991).

[24] G. L. R. Mair and R. G. Forbes, Surf. Sci. **266**, 180 (1992).

[25] P. T. Kirstein, G. S. Kino, and W. E. Waters, *Space-Charge Flow* (McGraw-Hill, New York, 1967).

[26] J. M. Finn, T. M. Antonsen, and W. M. Manheimer, IEEE Trans. Plasma Sci. **16**, 281 (1988).

[27] G. S. Boltachev and N. M. Zubarev, Europhys. Lett. **76**, 36 (2006).

[28] L. Landau and E. Lifshitz, *Fluid Mechanics*, Course of Theoretical Physics (Pergamon, Oxford, 1987), Vol. 6.

[29] A. M. Ganan-Calvo, Phys. Rev. Lett. **79**, 217 (1997).

[30] A. Barrero, A. M. Ganan-Calvo, J. Davila, A. Palacios, and E. Gomez-Gonzalez, Phys. Rev. E **58**, 7309 (1998).

[31] A. Hirabayashi and J. F. de la Mora, Int. J. Mass Spectrom. Ion Process. **175**, 277 (1998).

[32] E. W. Muller, Phys. Rev. **102**, 618 (1956).